



Microstructure and wear resistance of laser clad Inconel 625 and Colmonoy 6 depositions on Inconel 625 substrate

N. Jeyaprakash¹ · Che-Hua Yang^{1,2} · K. R. Ramkumar³

Received: 4 November 2019 / Accepted: 15 May 2020 / Published online: 26 May 2020
© Springer-Verlag GmbH Germany, part of Springer Nature 2020

Abstract

Nickel-based alloy Inconel 625 is used in higher mechanical stress applications because of their superior oxidation and creep resistance. However, their undesirable tribological behaviour is the major technical issues in several applications. This research carried out the comparative investigation of Inconel 625 (IN625) and Colmonoy 6 deposition over IN625 substrate by laser cladding technique. The metallurgical, mechanical and tribological properties were investigated. Results showed that the presence of hard laves and γ -Ni phases were observed on Colmonoy 6 and IN625 clad surface, respectively. Besides, Colmonoy 6 clad contains more than 60% of the hard laves phase which has capable of providing higher hardness and wear resistance. The hard laves phase and higher hardness in Colmonoy 6 clad provided a strong network to enhance the wear resistance and reduced the roughness average compared to IN625 clad and base material. The Colmonoy 6 clad was the promising one for the sliding components to resist the sliding wear.

Keywords IN625 · Colmonoy 6 · Laser cladding · Microstructure · Wear mechanism · Adhesive · Delamination · Roughness

1 Introduction

An advanced technique like laser cladding uses for the development of protective layers over the substrate either cladding the same substrate material or different material [1]. Owing to the irradiation of a high-power laser beam, the deposited powder particles bonded firmly fused with base metal [2]. However, the other surface modification techniques such as tungsten inert gas (TIG), electron beam and thermal spray were used to improve the surface properties [3].

Based on the previous observation, the conventional-based TIG process produces crack due to induced residual stress [4]; electron-based surface modification are expensive and needs higher initial investment; thermal spray-based coating process shows lesser bond strength which is unfit for wear resistance application [5]. There are some metals or alloys that undergoes failure in service condition due to long run usage. Therefore, it is necessary to forecast the failure in advance otherwise the material removal may increase the possibility for catastrophic consequences. It is a prerequisite to improve the wear resistance of dynamic parts to evade material removal and service life extension. Improvement in wear resistance leads to a reduction in failure, the stability of shape, resistance to impact and sliding load of movable components [5].

The hard facing alloy particles such as iron, cobalt, titanium and nickel are used in many applications due to its higher hardness. Among those alloy particles, nickel-based alloy powder Inconel 625 (IN625) possesses excellent corrosion and oxidation resistance. The matrix phase Ni–Cr is strengthened by molybdenum and niobium addition, which causes solid solution strengthening to maintain high strength and toughness up to 1093 °C. With the presence of high Ni content, IN625 inhibits stress-corrosion cracking and pitting corrosion, which

✉ N. Jeyaprakash
prakash84gct@gmail.com; prakash@ntut.edu.tw

Che-Hua Yang
chyang@ntut.edu.tw

K. R. Ramkumar
get2raam@gmail.com

¹ Centre of Mass Customization Additive Manufacture, National Taipei University of Technology, Taipei 10608, Taiwan, ROC

² Institute of Manufacturing Technology, National Taipei University of Technology, Taipei 10608, Taiwan, ROC

³ Department of Metallurgical and Materials Engineering, Indian Institute of Technology Madras, Chennai, India

is using in heat exchangers and fasteners [6–8]. Colmonoy grades belong to Ni-based superalloys which can potentially replace the cobalt-based alloys, as it provides sufficient adhesive and abrasive wear resistance, owing to the presence of higher chromium and boron content. Colmonoy alloys have higher hardness than Stellite alloys due to the presence of chromium carbides and chromium borides content in the substance [9]. The presence of iron and chromium in the mixture influences the alloying effect at both room temperature and elevated temperature and inhibits the related effect on the stacking fault energy. In general, Ni matrix has higher stacking fault energy (SFE) than the cobalt matrix, which results in the increase in the tendency to cross slip and galling, thereby undesirably affects the tribological property of the specimen [10, 11].

The laser alloying with WC–Co particle on the nodular iron surface was performed and concluded that wear resistance was improved with reasonable hardness [12]. The corrosion resistance of zircaloy with niobium coated laser alloying was examined and the results indicated that the treated surface improved the corrosion resistance due to the combined solution of refined microstructure with Nb elements [13]. The wear resistance of Ti–Cu–N laser cladding on the Ti substrate was investigated and their corresponding results showed that wear resistance was improved significantly and friction force depends on Cu addition in the coating [14]. TiC was reinforced on Ti–Al–Si using laser coating on TC4 alloy and indicated that microhardness and coating wear properties was improved due to refined microstructure [15]. The CrC–NiCr particle were alloyed on cast iron surface and concluded that noticeable wear resistant was observed on treated surface. Further, various wear mechanisms such as abrasive, adhesive and delamination were noticed while increasing the sliding distance [16]. The tribological properties of iron-based laser coating on steel metal were studied and stated that the coating surface providing a better protective layer against corrosion [17].

However, there is no research work conducted in comparison of IN625 and Colmonoy 6 clad on IN625 substrate through the laser cladding technique. In this work, advanced microscopic techniques were used to analyse the cladding thickness and its interfacial morphologies. Besides, hardness and dry sliding wear behaviour test were conducted on the cladding specimen and compared with the as received IN625 base material. The worn surface morphologies were analysed through the SEM technique, and the surface roughness was measured over the worn surface to find out the smoothness of the surface.

2 Experimental procedure

Commercially available IN625 was used as a substrate material and the cladding materials are IN625 and Colmonoy 6 particles. Table 1 shows the chemical composition of cladding materials. Initially, surface of IN625 was cleaned using SiC emery sheets. The surface was kept rough and hard to get superior bonding by the interlocking of powder particles with the substrate. Then, the surface was processed with high power 6 kW Yb: YAG disk laser beam. The wavelength of the laser beam was about 1030 nm, and circular shape beam mode was applied. The deposition rate was kept 600 μm thickness. The dimensions of the substrate were 100 mm in length and 50 mm in breadth and 20 mm of width. Figure 1 shows the schematic illustration of the laser cladding process. Figure 2a, b shows the SEM micrographs of IN625 and Colmonoy 6 particles, respectively, and the measured particle size of IN625 and Colmonoy 6 were $88 \pm 04 \mu\text{m}$ and $73 \pm 06 \mu\text{m}$. The size of the particles was measured using Image J software through linear intercept method. The parameters were opted by varying the power (W), scanning speed (mm/min) and feed rate (g/min), i.e. trial and error method. Table 2 depicts the process parameter used for the laser cladding process.

After cladding, the specimens were taken out by machining using wire electrical discharge machining (EDM) process for the required dimension. The specimen of $20 \times 20 \times 20 \text{ mm}$ was machined out for XRD and microscopic analysis. The specimens were etched from SiC emery

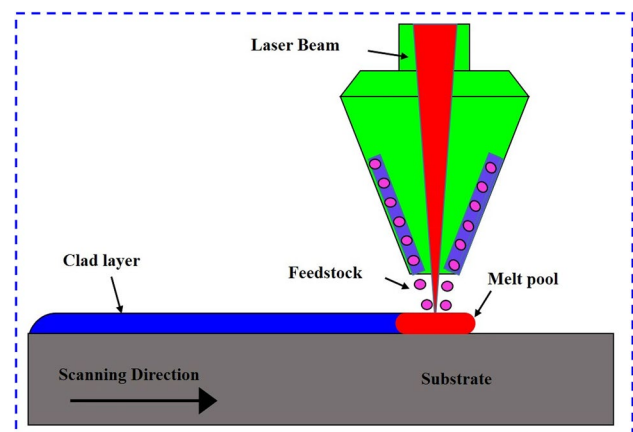


Fig. 1 Schematic representation of Laser cladding system

Table 1 Chemical composition of the coating materials

Materials	Ni	Co	Cr	Fe	B	Si	C	Mn	Mo	Nb
Colmonoy 6	REM	0.09	14.65	3.64	3.44	4.54	0.83	–	–	–
Inconel 625	REM		21.2	0.68		0.46	0.13	0.36	8.67	3.53

sheets of grit size 340–3000 GSM followed by diamond polishing on the polished surface. The etchants used after polishing was 2% chromic acid solution through the electrolytic technique. The specimens were polished over the cladding surface and in the cross section of the surface to analyse the morphological behaviour and interfacial behaviour, respectively. Vickers hardness test was conducted to check the hardness in the cross-sectional area from top to bottom of the clad specimen. The indentation marks were captured using optical microscopy to ensure the size of the indentation mark and crack nucleation or propagation. Further, ball on disc wear study was conducted on both laser cladding and base material surface to evaluate the tribological properties. Hardened tungsten carbide balls were used as a counterpart. For every test, the sample (disc) weight was measured before and after the test to measure the difference in mass loss. The parameters used for wear study were 40 N load, 1 m/s velocity and 2500 m sliding distance. After the wear test,

worn out surfaces were studied to identify the various wear mechanisms. Besides, the corresponding roughness average was measured using whitelight interferometer. The equipment handled for characterization, mechanical study, wear analysis and roughness measurement is given in Table 3.

3 Results and discussion

3.1 X-ray diffraction analysis

X-ray diffraction pattern of IN625 and Colmonoy 6 cladding surface is shown in Fig. 3a, b. In IN625 cladding, there were only γ -Ni peaks present over the cladding the surface which ensured that there was no intermetallic formation between the powder particles during cladding as shown in Fig. 3a [18]. On another side, it can be clearly noticed that the presence of the hard laves phase in the Colmonoy

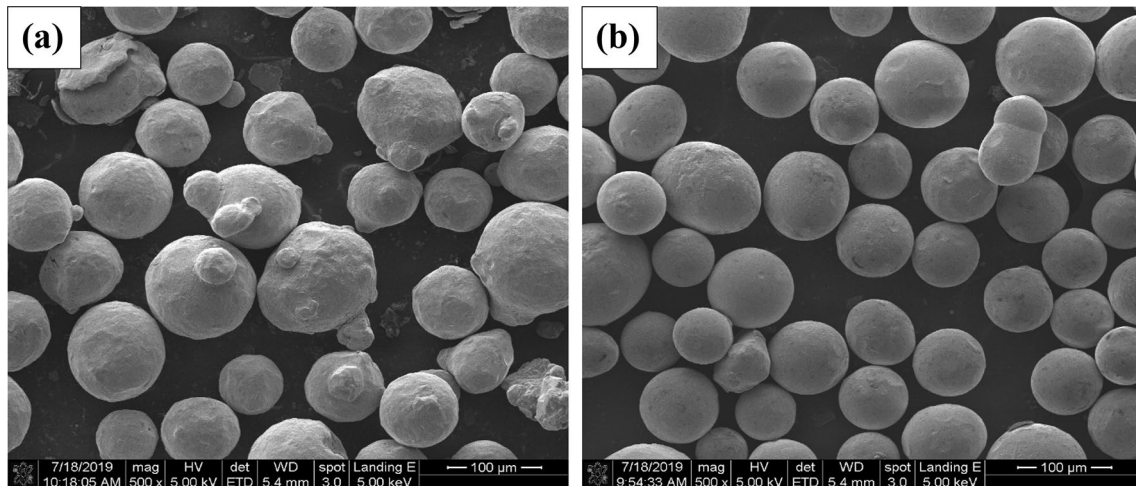


Fig. 2 SEM micrographs of as received powder particles: a IN625 and b Colmonoy-6

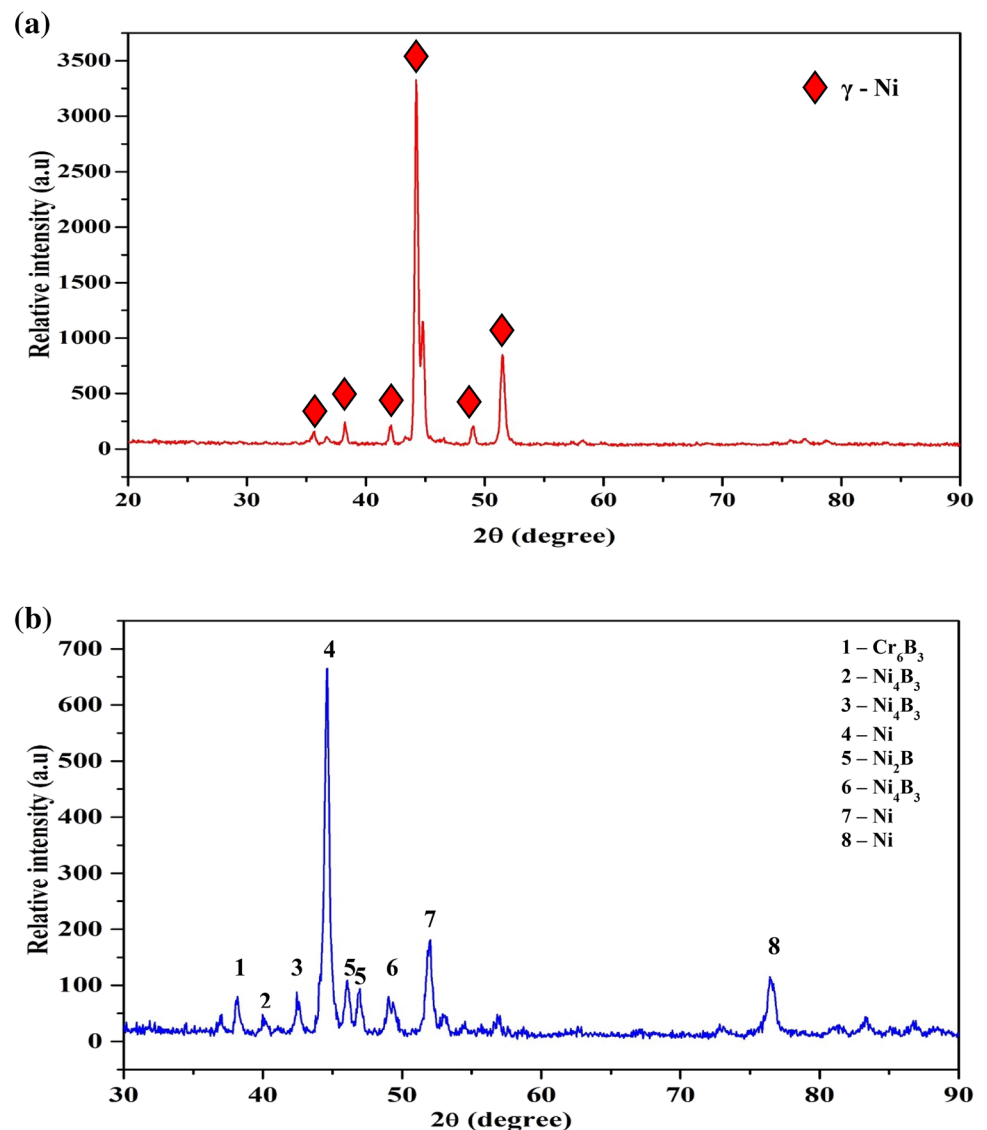
Table 2 Process parameter used for laser cladding

Plate grade	Speed (mm/min)	Feed rate (g/min)	Power (watts)	Powder carrier gas (argon)	Shielding gas (argon)	Pre heating (degrees)
Inconel 625	400	4	1000	6 SD @ 1 BAR	25 lpm	150

Table 3 Equipment utilised with process parameters

Name of the test	Equipment utilised (name and make)
XRD	Shimadzu XRD 6000, Japan, Cu α radiation, 30 mA and 40 kV
SEM with EDS	CARL ZEISS-SIGMAHV
Optical microscope	Dewinter Model- Dmi Victory
Hardness	Akashi MVK-H21, load of 300 g and dwell time of 20 s
Wear	High temperature and vacuum tribometer, M/s. Ducom Inc.
Surface roughness	Rtech Instruments, USA

Fig. 3 XRD pattern of **a** IN625, **b** Colmonoy 6 cladding



6 cladding specimen as shown in Fig. 3b. Laves phases are $(\text{FeNi})_3\text{B}$, Ni_3B and intermetallic compounds are Cr_7C_3 , Ni_4B_3 and Cr_{23}C_7 and CrB phase besides Ni phase on the cladding specimen. When compared with IN625, Colmonoy 6 retained as FCC even after cladding because Ni requires very high temperature (940°C) to transform into HCP structure. The temperature of IN625 is higher (1290°C) while compared to Colmonoy 6. Hence, XRD results helped to analyse the presence of phases in the microstructure of the clad [19].

3.2 Microscopy examination

Microscopy images were captured over the surface of the coatings and interface to understand the morphologies of the clad specimen. Figure 4a, b shows the optical images of IN625 cladding cross section with interface region and

cladding region, respectively. It can be noticed from the micrograph that there were no defects such as pores or cracks in the cladding regions. In the laser cladding technique, the heat source was controlled properly by optimizing the laser parameters. Hence, the possibility of defects has been avoided [20]. Figure 4a shows the various microstructure from the cladding region to substrate material. The formed structures are coaxial dendrites, columnar and cellular dendrites as represented in Fig. 4a, c. In the interface region and near the interface, the observed structure was cellular. Because of constitutional undercooling, the dendritic structure was formed. During the solidification period, the melt pool in the cooling front develops rich alloy elements in the coating. The gradient temperature was reduced and the rate of growth has improved from the melt region into near coating region [21]. The dendrites orientation indicates that the temperature is transferred over the base material; thus

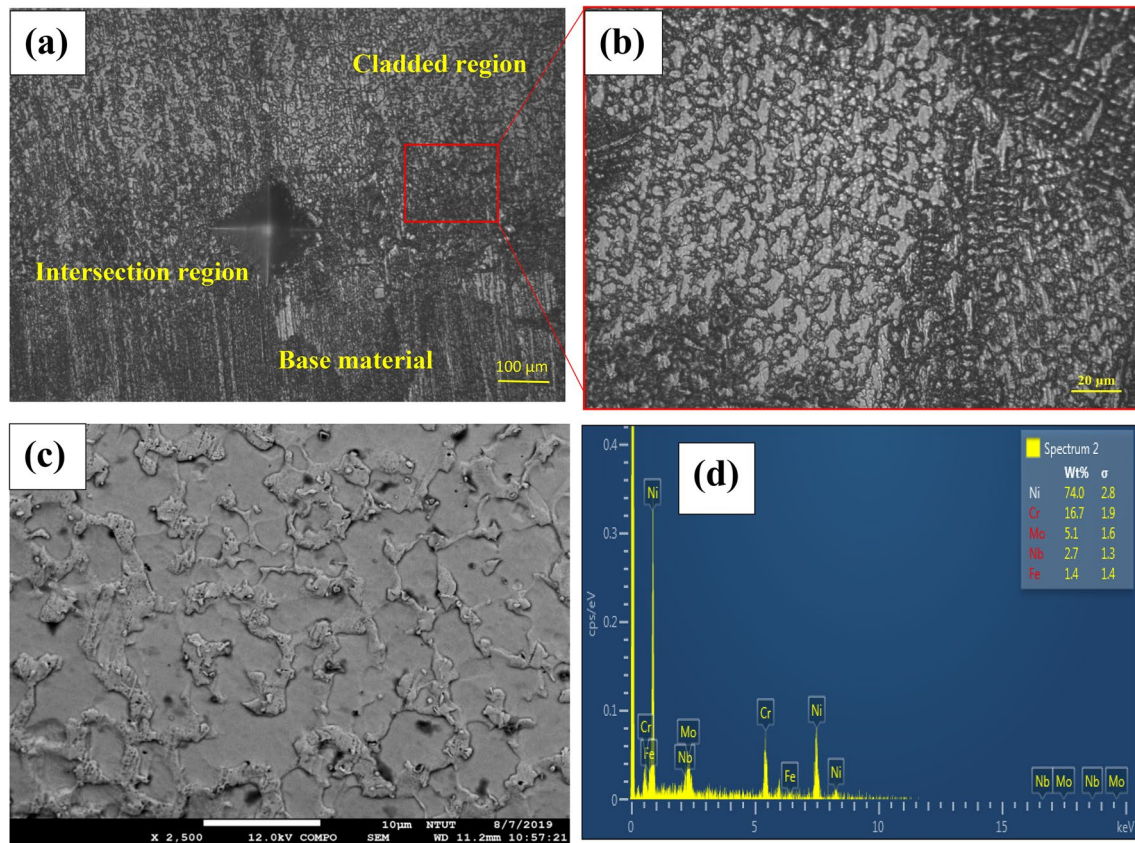


Fig. 4 Optical micrograph of IN625 cladding cross section with various zone (a), Cladding region with various structures (b), FE-SEM micrographs over the center of the specimen after coating (c) and the corresponding EDS of (c) is shown in d

the flow heat direction is perpendicular to the base metal surface during cooling period, which creates the directional dendritic structure to be formed [22]. Generally, the cooling amount is greater in the melt pool region and the same time, the rate of cooling decreases in the direction of coating surface. So, there is no possibility to form the secondary arms in the bottom region of melt pool and the formed structure is cellular. The primary structure such as soft Ni matrix and γ -Ni phase is obtained in IN625 clad surface as shown in Fig. 4c.

Metallographic study was conducted on the cross-sectioned Colmonoy 6 cladding surface (Fig. 5a, d). No defects were observed on the cladding surface. The noticed microstructure indicate that uniform dendrite towards a build-up direction. The observed phases between γ -nickel were eutectic phases. The darker region represents boride content, and lighter regions indicate γ -nickel. In Colmonoy 6 clad region, a large amount of intermetallic laves phase was formed over the clad surface as shown in Fig. 5a, c. The laves phase was $(\text{FeNi})_3\text{B}$ and Ni_3B which was ensured through XRD analysis. Almost more than half of the surface contains laves phase which promises to enhance the load carrying capacity of the material [23]. Additionally, the intermetallic

compounds, namely CrB , Cr_7C_3 , Ni_4B_3 and Cr_{23}C_7 were expected to improve the strength of the material because there were no needle-like structures that were found which ensures the presence of intermetallic phases helps for property enhancement. The CrB phase was present in the clad and helps to resist the crack nucleation in the system. Both the IN625 and Colmonoy 6 clad were bonded highly due to moderate heat input without any defects such as porosity and cracks [24]. Figures 4d and 5d shows the EDS analysis conducted over the IN625 and Colmonoy 6 clad surface. From Fig. 4d, the primary element present in the system is Ni followed to Cr, Mo, Nb and Fe. In Fig. 5d, the identified major percentage of element is Ni and followed by Cr, Mo, Si, O, and Fe. The obtained results are indicating that all the elements were distributed throughout the cladded surface and produced the strong network against material loss. Further, it is necessary to investigate the interfacial behaviour of the cladding. Sometimes, clad layer may delaminate or exfoliate owing to poor bonding with the base metal. In addition, there was a possibility to peel off coating layer due to mismatch of thermal expansion coefficient under cooling period. After cladding, there is a chances for nucleation of cracks if it brittle due to the presence of intermetallic compounds.

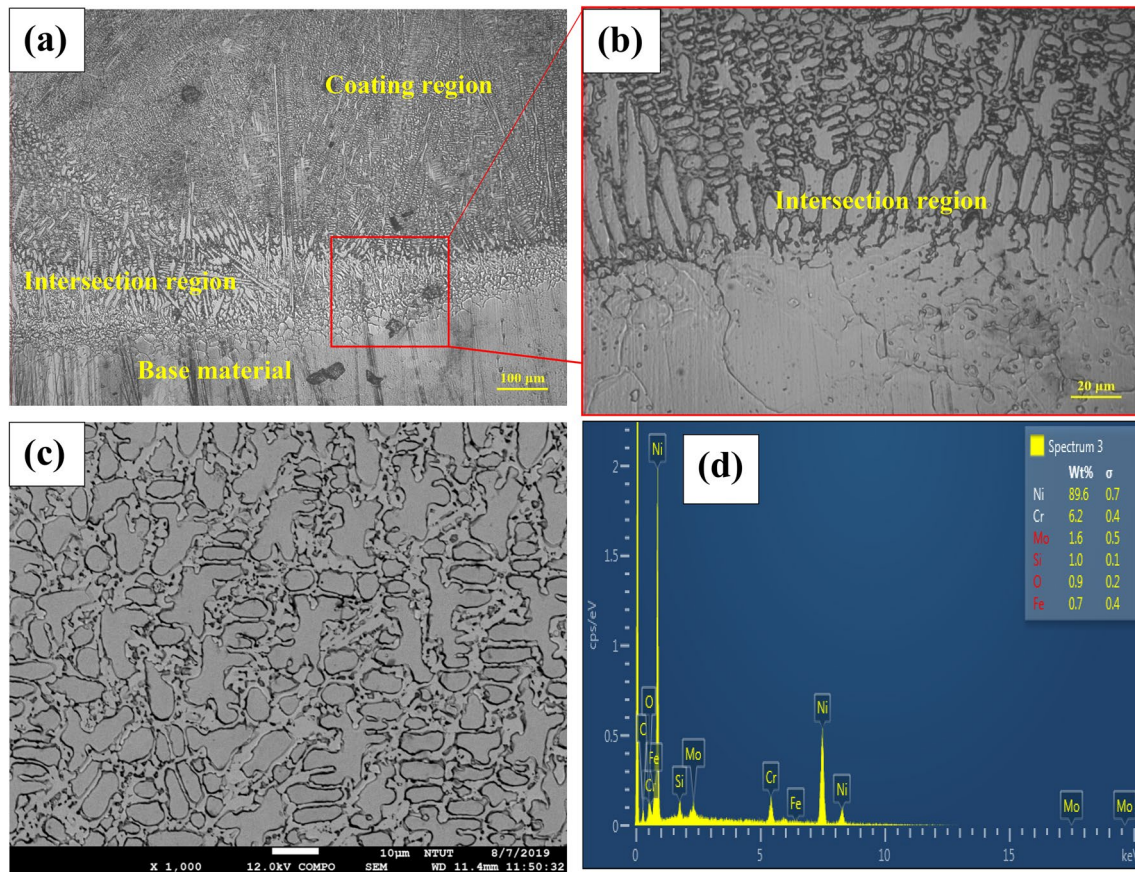


Fig. 5 Optical micrograph of Colmonoy 6 coating cross section with various region (a), magnified view of intersection region with various structures (b), FE-SEM micrographs over the center of the specimen after coating (c), corresponding elemental analysis (d)

Here, the average thickness of interfacial layer of IN625 and Colmonoy 6 are $112.51 \pm 04 \mu\text{m}$ and $78.38 \pm 07 \mu\text{m}$, respectively (Figs. 4a, 5b). The thickness of the interface layer was very thin in Colmonoy 6 clad compared to IN625 clad sample. As both of the clad are Ni-based superalloys and it has laves phases in the structure. The Colmonoy 6 has higher amount of laves phases fraction compared with IN625 clad. Hence, in accordance with the thickness of the interface and laves phase fraction, the possibilities for cracking is prone to occur in IN625 coated sample than Colmonoy 6 clad. Furthermore, Colmonoy 6 coated specimen contains more than 60% of hard laves phase in the cross section of the coating (measured using Image J software in threshold condition) which has capable of providing higher hardness and wear resistance [23, 24].

3.3 Microhardness test

Hardness is a substantial property influence the wear resistance of the material. Thus, the Vickers' microhardness test was conducted in the cross section of the specimen in cladding zone, interfacial zone and base metal (Fig. 6a, b).

Figure 6a depicts the schematic representation of the place where their indenter loaded. The hardness of the Colmonoy 6 clad specimen was higher than IN625 cladding in both the cladding zone and interfacial zone. In Colmonoy 6 clad specimen, the average hardness values obtained in the clad and interface are 671.5 HV and 300.2 HV, respectively. In IN625 clad, the average hardness values obtained in the clad and interface are 469.8 HV and 235.5 HV, respectively. In as-received condition, the hardness of the IN625 was 280.72 HV. The hardness obtained in the cladding zone of Colmonoy 6 is twice higher than the base metal. The increase in hardness values is due to the presence of laves phase in the soft matrix and defect-free cladding. Also, the improved hardness on the clad surface due to proper fusion of alloy particles to base material. The decrease in hardness values in IN625 was due to a lack of laves phase and the absence of strong intermetallic phases in the matrix [25]. In addition, the inset SEM images depict that the indentation marks occurred during testing. The size of indentation is small in the cladding zone and interfacial zone of the Colmonoy 6 clad specimen whereas it is large in both zones in IN625 clad sample. The smaller sized marks reveal that

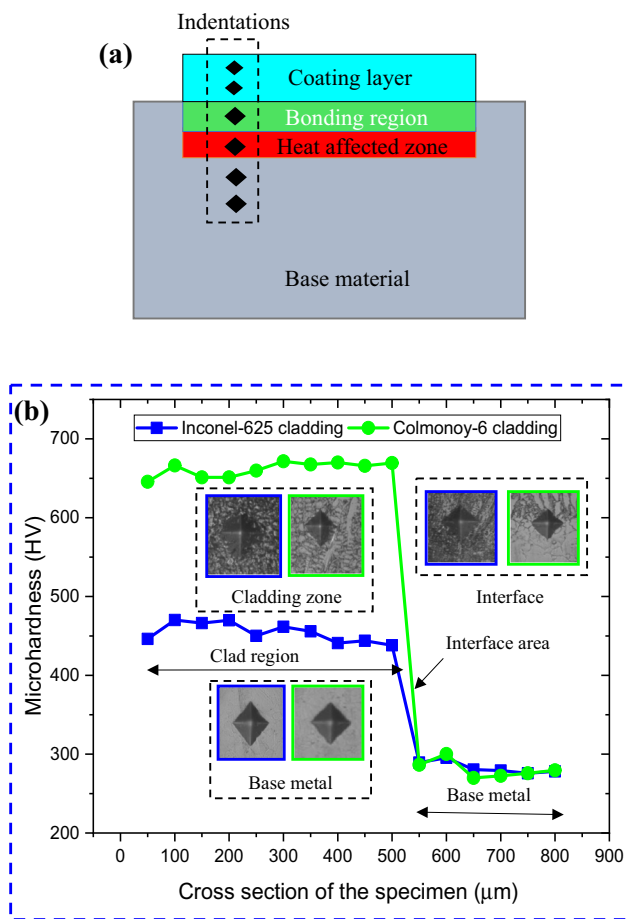


Fig. 6 Schematic representation of various region with indentations (a), microhardness profile of various regions of the coated specimens (b) (Insets show the indentation mark in particular place of the zone)

the clad has capable of withstanding higher loads when compared with larger marks when applying the same load in both the clads.

3.4 Dry sliding wear behaviour

The measured values of the friction coefficient were drawn as a function of sliding distance for all the three samples. Figure 7a shows the friction coefficient graph of substrate, Colmonoy 6 and IN625 clad specimens. In the starting stage of the test, the tribological system was followed a transient friction regime for the distance of 500 m nearly, then friction shows with steady state for the remaining distance and all the three samples show the same tendency. When sliding distance increases, the coefficient of friction (CoF) also increases due to reduced adhesion resistance. The reason for increasing the friction force is due to locally increasing the heat between contact points. The another chance for increased CoF is the adhesion resistance which is related to the adherence or magnetism of the contact surfaces. In sliding wear study, relative motion occurs in the two contact pairs and prevents the move against each other. It can be observed that the CoF of the un-cladding specimen is more than cladding specimens. This may be due to the adhesion effect of the base material during wear study. All the three specimens show higher CoF in the beginning, then reduced while increasing sliding distance. In the start stage of the test, the distributed asperities between the surfaces were hard and sharp, when counterpart sliding over the specimen surfaces the CoF is higher. After sliding some meters, the contact surfaces got even by removing the uneven surfaces and burrs, and caused stable in CoF. The CoF values of the substrate, IN625 and Colmonoy 6 cladding specimens are 0.65, 0.65 and 0.53, respectively. The lower CoF values obtained in Colmonoy 6 clad specimen due to the

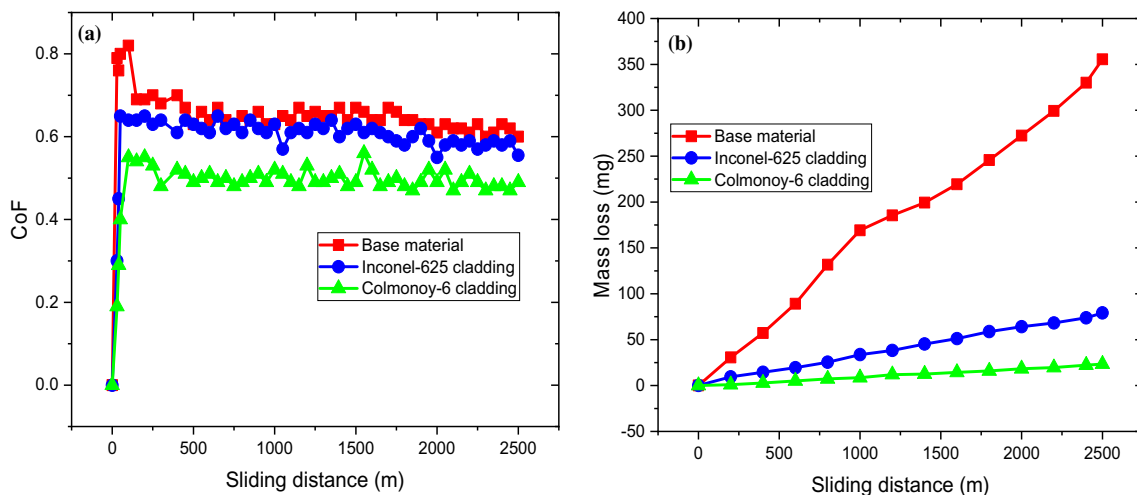


Fig. 7 Tribological behaviour of base metal and laser cladding specimen a CoF, b Mass loss

microstructure, i.e. the presence of hard laves phases. This structure condenses the generation of crack and reducing the cracks rate diffusion. Then, the wear rate is also an important factor in the reduction of CoF values besides hardness [26].

Figure 7b depicts the mass loss occurred in the base material, IN625 and Colmonoy 6 clad specimens after dry sliding wear behaviour analysis. From Fig. 7b, it can be a clear understanding that the Colmonoy 6 clad specimen undergone very lower mass loss when compared with IN625 clad sample. With respect to sliding distance from 200 to 1200 m, the mass loss was 9.51–79.18 mg in IN625 clad specimen and 0.99–23.53 mg in Colmonoy 6 cladding specimen. According to Archard's wear law, mass loss is directly proportional to the applied load and travelled distance, inversely proportional to the material hardness. The obtained results specify that wear resistance was highly correlated with their respective hardness [27]. In addition to that, the base material shows poor wear resistance compared to cladding specimens due to lesser hardness.

3.5 Wear mechanism and roughness measurement

The worn-out morphology of base material after the ball on disc wear study is shown in Fig. 8a. It can be observed that the wear intensity of base material is higher when compared to laser cladding samples. The plough marks were noticed on the worn-out surface of base material and this represents the higher plastic deformation and lesser wear resistance to abrasion [28]. The material removal rate shows higher than laser cladding specimens. The observed wear mechanisms on the worn-out base material are micro ploughing, deep grooves, abrasive and delaminations. The higher frictional force causes plastic deformation and severe damages as the sliding distance increases. The wear debris and uneven portion can be observed on the base worn out surface, producing over the shear stresses working on the surfaces [29]. The continuous sliding produces plate like pieces due to plastic deformation and repeatedly it produces plate like

morphology. From the observed wear morphologies, adhesion and delamination was dominated than other mechanism on the base worn out surfaces [30]. The corresponding roughness average shows around 4.9 microns. Figure 8b, c shows the base metal worn surface of 3D topography and their corresponding roughness average, respectively. The poor wear resistance and lesser hardness are reflected in the roughness of base material.

Figure 9a indicates the wear morphologies of IN625 laser cladding specimen. It is noticeable that the wear morphologies were relatively different from the base material. It is confirmed over measured frictional force through a tribometer. In general, there are mild abrasive and adhesive wear mechanisms were noticed on the worn surfaces. In Fig. 9a, mild wear tracks, scratches, and grooves were noticed in various places even in magnified image which reveals, occurred wear was adhesive owing to its moderate hardness level. Due to moderate hardness and wear resistance, the mating disc excavated the material from the IN625 cladding. Hence, mild wear tracks could be obtained on the worn-out surfaces. Further, the wear track of IN625 clad shows shallower when compared with the base material. Besides, oxidation also was noticed on the worn surface due to higher frictional heating. While slides counter ball on the surface, the harder semi-molten wear debris fell off because of weak interconnection. Then, the hard wear debris fell off and mild craters were formed. Further, the narrow continuous wear track creates the micro-cutting, which represents that abrasive is dominant wear. Figure 9b, c shows the IN625 clad worn surface of 3D topography and their corresponding roughness average, respectively. The IN625 wear surface shows lesser surface roughness of 2.4 μm compared to the base material. This was due to moderate hardness and material loss of cladding surface. Figure 10a represents the worn-out surface of Colmonoy 6 cladding. The obtained wear mechanism was abrasive wear which was ensured through distributed debris particle over the surface. There were wear tracks that could be identified which were not so deep like

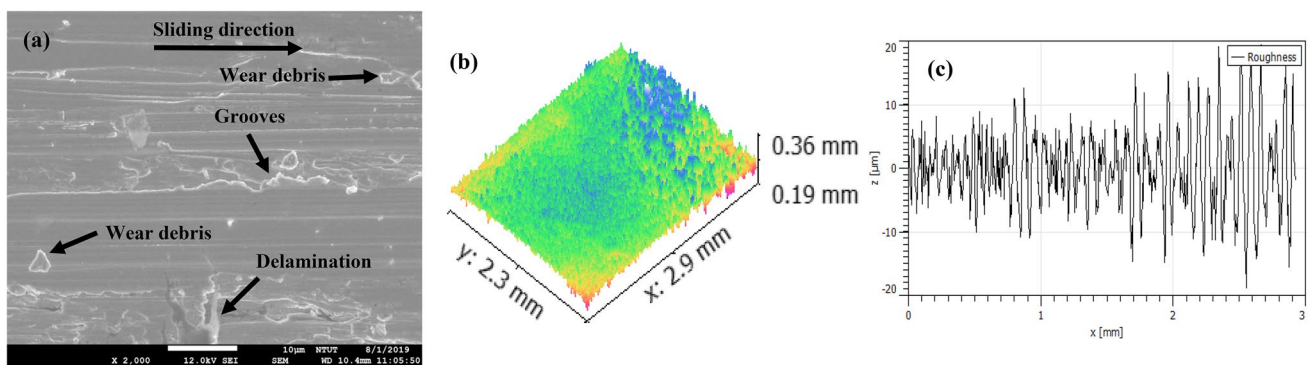


Fig. 8 Base material; **a** micrograph of worn out surface; **b** 3D topography of worn surface; and its corresponding roughness average (**c**)

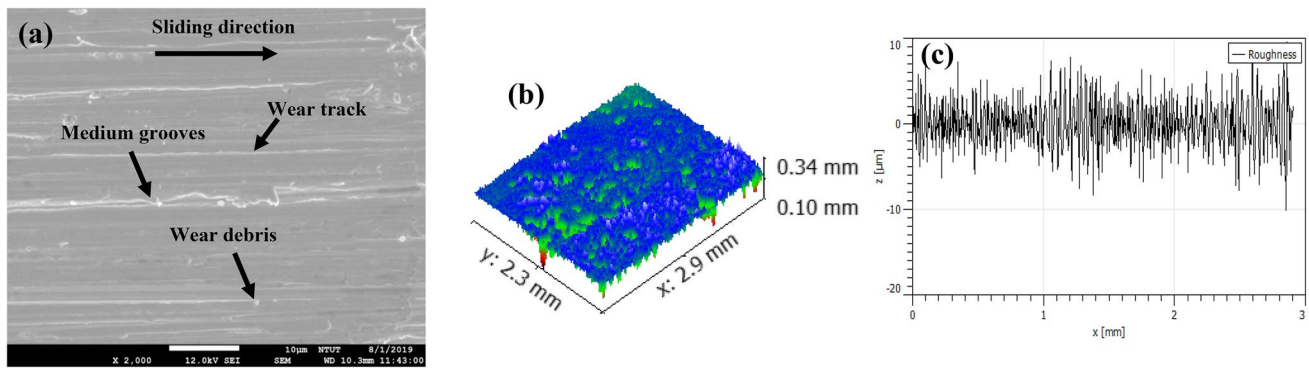


Fig. 9 IN625 cladding; **a** micrograph of worn out surface; **b** 3D topography of worn surface; and its corresponding roughness average (**c**)

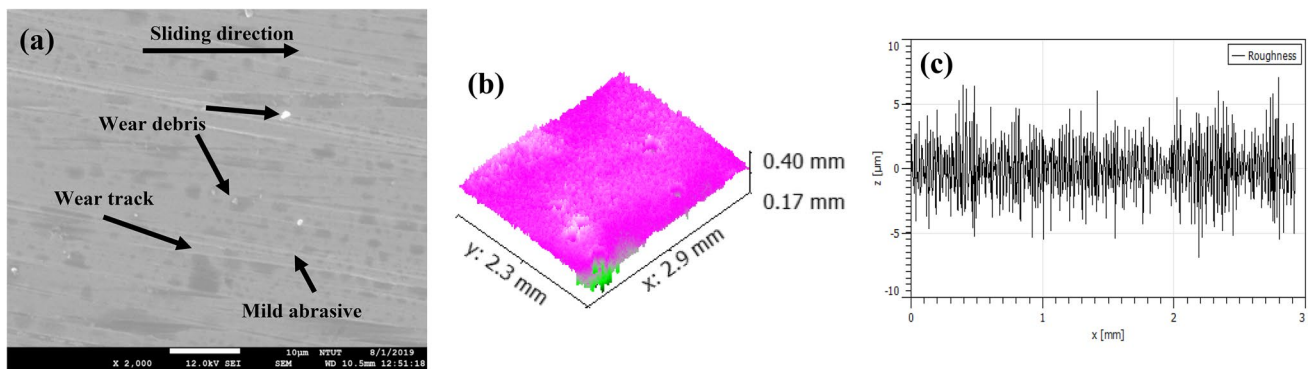


Fig. 10 Colmonoy 6 cladding; **a** micrograph of worn out surface; **b** 3D topography of worn surface; and its corresponding roughness average (**c**)

tracks occurred in the substrate. The reason for lesser wear tracks and absence of severe wear was due to higher hardness provided by the Colmonoy 6 clad layer. Besides, few grooves could be noticed in the magnified image. At last, in Colmonoy 6 clad specimen, there were only traces for wear tracks in the specimen with very few debris particles which confirms that the hardness and wear resistance were highly correlated with each other according to Archard's wear law [25–27]. The formation of wear debris, wear track and micro-cutting has a close connection with wear mechanism of examined samples. Based on the investigation of worn-out surfaces, the base material shown severe adhesive and delamination while cladding specimens suffered from mild abrasive wear. The study on the wear behaviour of Colmonoy 6 cladding can form a strong network to protect the surface from a severe wear atmosphere. The plastic deformation and micro ploughing is not noticed on the cladding surface by making grooves. The Colmonoy 6 clad specimen surface shows the lower roughness $1.8 \mu\text{m}$. Figure 10b, c shows the Colmonoy 6 clad worn surface of 3D topography and their corresponding roughness average, respectively. The hard laves phase and higher hardness in Colmonoy 6 clad provided a strong network to enhance the wear resistance and reduced

the roughness average. Figure 11 shows the schematic representation of the wear mechanism that occurred. Figure 11a) shows the various failures occurred during wear test in the base material. Particle pulls out, delamination, plastic deformation, grooves were pointed out. Figure 11b) indicates the IN625 clad and represents that IN625 clad can resist the deformation of wear. At last, Fig. 11c) wear has been drastically reduced by depositing Colmonoy 6 powder particles. Only wear debris, wear tracks and fine grooves were identified in SEM morphology which has been mirrored in the schematic. Based on the obtained result, Colmonoy 6 clad will be the promising one for the sliding components to resist the sliding wear.

4 Conclusion

IN625 cladding showed only γ -Ni peaks over the cladding surface while Colmonoy 6 showed Laves phases such as $(\text{FeNi})_3\text{B}$, Ni_3B and intermetallic compounds such as Cr_7C_3 , Ni_4B_3 , Cr_{23}C_7 and CrB phase. The primary structure such as soft Ni matrix and γ -Ni phase was obtained in IN625 clad surface and a large amount of intermetallic laves phase

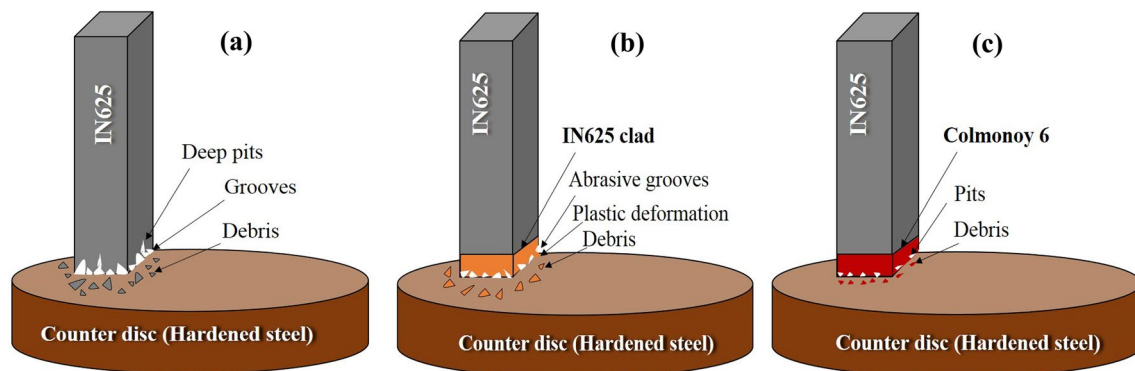


Fig. 11 Schematic illustration of wear mechanism occurred in this wear study: **a** severe wear failure after DSWB analysis (before cladding), **b** IN625 cladding shows with mild abrasive and plastic deformation, **c** Colmonoy 6 cladding specimen shows with small groove

was formed over the Colmonoy clad surface. Besides, Colmonoy 6 coated specimen showed more than 60% of hard laves phase in the cross section of the coating which proved with higher hardness, compressive strength and wear resistance. The hardness obtained in the cladding zone of Colmonoy 6 was higher than the base metal and IN625 clad due to the presence of the laves phase. The CoF of the uncladding specimen was more than cladding specimens due to the adhesion effect of the base material during wear study. Besides, the Colmonoy 6 clad specimen undergone a very lower mass loss when compared with IN625 clad sample. According to Archard's wear law, the obtained mass loss was directly proportional to the applied load and travelled distance, inversely proportional to the material hardness. Based on the investigation of worn-out surfaces, the base material showed severe adhesive and delamination while cladding specimens suffered from mild abrasive wear. The hard laves phase and higher hardness in Colmonoy 6 clad provided a strong network to enhance the wear resistance and reduced the roughness average. Based on the obtained result, Colmonoy 6 clad was the promising one for the sliding components to resist the sliding wear.

Acknowledgements Author's wishes to thank Ministry of Science and Technology (MOST), Taiwan, ROC for providing financial support to carry out this research work.

References

1. R. Maestracci, A. Sova, M. Jeandin, J.M. Malhaire, I. Movchan, Ph Bertrand, I. Smurov, *Surface Coat. Technol.* **287**, 1 (2016)
2. Sarka Houdkova, Zdenek Pala, Eva Smazalova, Marek Vostrak, Zdenek Cesanek, *Surface Coat. Technol.* **318**, 129 (2017)
3. N. Jeyaprakash, C.-H. Yang, M. Duraiselvam, S. Sivasankaran, *Arch. Civ. Mech. Eng.* **20**, 20 (2020). <https://doi.org/10.1007/s43452-020-00030-4>
4. M.H. Sohi, M. Ebrahimi, H.M. Ghasemi, A. Shahripour, *Appl. Surf. Sci.* **258**, 7348 (2012)
5. P. Fauchais, G. Montavon, *Adv. Heat Transf.* **40**, 205 (2007)
6. H.R. Rezaei Ashtiani, R. Zarandooz, *Int. J. Adv. Manuf. Technol.* **84**, 607 (2015)
7. S.S. Sandhu, A.S. Shahi, *J. Mater. Process. Technol.* **233**, 1 (2016)
8. D. Verdi, M.A. Garrido, C.J. Múñez, P. Poza, *Mater. Des.* **67**, 20 (2015)
9. V. Ramasubbu, G. Chakraborty, S.K. Albert, A.K. Bhaduri, *Mater. Sci. Technol.* **27**, 573 (2011)
10. L.J. da Silva, A. Sofia, A. Oliveira, *Wear* **350**, 130 (2016)
11. I. Hemmati, V. Ocelik, K. Csach, J.T.M. De Hosson, *Metall. Mater. Trans. A* **45**, 878 (2013)
12. N. Jeyaprakash, M. Duraiselvam, S.V. Aditya, *Surface Rev. Lett.* **25**, 7 (2018)
13. Sung-Joon Lee, Hyuk-Sang Kwon, Joung-Soo Kim, *Met. Mater.* **6**, 145 (2000)
14. Yuling Yang, Shiyin Cao, Shuai Zhang, Xu Chuan, Gaowu Qin, *Appl. Phys. A* **123**, 474 (2017)
15. H.X. Zhang, J.J. Dai, Z.W. Ma, X.Y. Wang, N.L. Zhang, *Surf. Rev. Lett.* (2019). <https://doi.org/10.1142/S0218625X1950077X>
16. N. Jeyaprakash, M. Duraiselvam, R. Raju, *Arch. Metall. Mater.* **63**, 1303 (2018)
17. Li Fan, Hai-yan Chen, Yao-hua Dong, Li-hua Dong, Yan-sheng Yin, *Int. J. Miner. Metall. Mater.* **25**, 716 (2018)
18. T.E. Abioye, D.G. McCartney, A.T. Clare, *J. Mater. Process. Technol.* **217**, 232 (2015)
19. C.P. Paula, A. Jainb, P. Ganesha, J. Negic, A.K. Nath, *Opt. Lasers Eng.* **44**, 1096 (2006)
20. M.N. Fesharakia, R. Shoja-Razavi, H.A. Mansouri, H. Jamali, *Surface Coat. Technol.* **353**, 25 (2018)
21. S. Kou, *Welding Metallurgy* (Wiley, Hoboken, 2017)
22. T.E. Abioye, J. Folkes, A.T. Clare, *J. Mater. Process. Technol.* **217**, 232 (2015)
23. K. Feng, Y. Chai, P. Deng, Y. Li, H. Zhao, F. Lu, R. Li, J. Huang, Z. Li, *J. Mater. Process. Technol.* **243**, 82 (2017)
24. S. Gnanasekaran, G. Padmanaban, V. Balasubramanian, *High Temp. Mater. Process. (Lond.)* **38**, 16 (2019)
25. M. Miguel, J.M. Guilemany, S. Vizcaino, *Tribol. Int.* **36**, 181 (2003)
26. C. Guo, J. Zhou, J. Chen, J. Zhao, Y. Yu, H. Zhou, *Wear* **270**, 492 (2011)
27. R. González, M.A. García, I. Peñuelas, M. Cadenas, M.D.R. Fernández, A.H. Battez et al., *Wear* **263**, 619 (2007)
28. N. Jeyaprakash, C.-H. Yang, M. Duraiselvam, G. Prabu, *Results Phys.* **12**, 1610 (2019)

29. Chao Zheng, Yonghong Liu, Jie Qin, Renjie Ji, Shihong Zhang, J. Mech. Sci. Technol. **32**, 283 (2018)
30. C. Zheng, Y.H. Liu, H.X. Wang, J. Qin, S.H. Zhang, J. Mech. Sci. Technol. **31**, 625 (2017)

Publisher's Note Springer Nature remains neutral with regard to jurisdictional claims in published maps and institutional affiliations.